X-RAY MICRO-CT ASSISTED DRAINAGE ROCK TYPING FOR CHARACTERIZATION OF FLOW BEHAVIOUR OF LAMINATED SANDSTONE RESERVOIRS

Pradeep Bhattad[1], Benjamin Young[1], Carl Fredrik Berg[2], Alf Birger Rustad[2], Olivier Lopez[2]
(1) FEI Lithicon Digital Rock Services, Australia (2) Statoil AS, Norway

This paper was prepared for presentation at the International Symposium of the Society of Core Analysts held in Avignon, France, 8-11 September, 2014

ABSTRACT

Typically homogenous core plugs are preferred for routine and special core analysis (RCA and SCAL) programs, however many sandstone reservoirs are dominated by lamination on a sub-plug scale. In order to maximize the recovery of hydrocarbons from such systems, effective flow properties are needed, and these properties can be strongly influenced by the properties of tighter laminas. While anisotropy in flow properties for plugs (parallel and perpendicular to the laminations) might be used to estimate the flow properties of the different laminas present in the core plug; the accuracy of these estimates are dependent on the constituent rock-types and their spatial distribution within the plug.

In this study we demonstrate a novel method to study heterogeneous core plugs by first mapping heterogeneity within the plug and then determining flow behavior of each lamina at the sub-plug scale. Such lamina properties are critical to optimize k_v/k_h relationships and directional relative permeability for models of heterolithic reservoirs. The properties derived from an open and tight lamina were used as inputs in an upscaling exercise to obtain property at the core plug scale. Using proposed method, we accurately capture the spatial distribution of an open and tight rock and its effect on flow at the plug scale. Upscaled results show a good qualitative agreement with the experimental results measured on the same plugs.

INTRODUCTION

Numbers of formations on the Norwegian continental shelf (NCS) have interbedded deposits of sand and mud (heterolithic beddings). The thickness of these beddings is often below the log resolution and varies from millimeter to meter scale. To accurately model the fluid flow through heterogeneous reservoirs, it is crucial to characterize the spatial distribution of each rock unit [Jackson *et al.* 2003]. The rock types in the heterogeneous reservoir are defined by the reservoir engineers in two ways. The most commonly used method is based on the clustering of routine core properties such as porosity, permeability and formation factor [Archie 1952, Amaefule 1993] derived from a large number of core plugs. A less commonly used method, due to experimental time and cost, is based on the

multiphase flow behavior of a rock such as drainage [Hollis 2010] and relative permeability [Hamon 2004]. Both of these cases require homogenous samples, but for plugs in heterolithic formations it is rarely possible to have only one rock type per core plug. With recent developments in high resolution 3D imaging [Alberts 2013] and image based multiphase flow simulation techniques [Arns 2005, Lopez 2012], it is possible to acquire a detailed pore structure, and derive RCA and SCAL properties directly from the images. However, due to the limitation of sample size *vs.* image resolution, it is often not possible to resolve the connectivity of the throats and capture heterogeneity of the plugs in a single image. This also limits the analysis of the heterogeneous plugs using digital rock analysis. In this paper, we demonstrate a novel XCT assisted drainage rock typing method to map a 3D spatial distribution of constituent rock types on two highly laminated sandstones plugs from the NCS. We use multi-resolution CT imaging and image registration techniques to capture both, the heterogeneity at the plug scale, and resolve throat connectivity.

MATERIALS AND METHODS

Two highly laminated sandstone plugs, sample 235 and 254, from the NCS were chosen for this study. Visually, both plugs consist of at least two rock types: open (lighter color) and tight (darker color), as seen in figure 1. Both samples have horizontal beddings. Sample 235 contains mainly a tight lamina, while sample 254 contains mainly an open lamina.

The plugs in dry state were imaged using XCT (resolution ~15μm/voxel) for investigation of rock type distribution. After imaging in dry state, the plugs were saturated under vacuum with X-ray attenuating brine (1M NaI-H_2O solution). The presence of the X-ray attenuating brine in the pores space increases the X-ray absorption, thus allowing us to quantify porosity of features below the image resolution. The dry (figure 2a) and saturated (figure 2b) state images were registered in a perfect geometric alignment [Latham et al. 2008], which enabled subtraction of the dry from the saturated image. The resulting difference is due to the presence of the X-ray dense brine in the pore-space, and in figure 2c one can see brighter regions corresponding to higher porosity. Such difference images are used to quantify total connected porosity, including porosity in features smaller than the image resolution using a "total connected porosity" segmentation technique [Ghous *et. al.*, 2007].

Using centrifuge we drained the X-ray attenuating brine from the fully saturated sample with air as a non-wetting fluid. The speed of the centrifuge was set to drain out only one rock type (4500 rmp, equivalent throat radius 3μm). The samples were not sleeved during the drainage to allow for the rock to drain from all sides irrespective of the layered nature of the plug. The plugs were then sealed in the imaging container to prevent drying and rested for 24 hours to allow the capillary forces to equilibrate before imaging the plug for the third time (figure 2d). In order to further investigate the properties of individual rock types at the pore scale, samples were cored into 3-5 mm diameter sub-plugs. Due to

difficulty in coring sub-plugs containing only one rock type, longer sub-plugs containing both rock types were cored; however digital analysis was performed on the subset of rock containing only the rock type of interest. Similar to the XCT imaging on the plugs, the sub-plugs were also imaged in the dry and the saturated state (resolution ~3μm), and thereafter registered. The sub-plugs were also registered to the exact location within each plug. This enabled a direct comparison of the segmented porosity estimates from both the plug and sub-plug images.

To investigate textures and secondary porosity below the resolution of the XCT images of the sub-plugs, 2D SEM imaging was carried out on a resin embedded polished section of the sub-plugs. The SEMs were registered into the 3D tomogram [Latham et al. 2008], thus allowing us to investigate the detailed structure of pores captured as sub-resolution porosity in the difference image. The polished sections were also analysed with QEMScan to quantify mineralogy of the sample. Porosity was measured using Helium pycnometry performed on the plug at the beginning of the study, and on the sister sub-plugs extracted to represent the different rock types. The sister sub-plugs were imaged in XCT to check whether it represented the same material as their sister samples. Afterwards the sister sub-plugs were used for mercury injection capillary pressure (MICP) experiments.

RESULTS AND DISCUSSION

Rock Typing

The XCT images of the dry samples revealed several rock types along the height of the plug; however we restricted this study to just two rock types: open and tight. The centrifuge speed was set at 4500 rpm corresponds to a hydraulic radius of 3 μm assumed to separate the two rock types. Due to the destructive nature of the MICP, the pore size distribution could not be obtained on the core plugs used in this study, and the 3μm cut-off size was chosen based on previous MICP observations on similar samples from this field. Figure 2d shows a registered image of the drained plug, areas where the X-ray attenuating brine has drained out during centrifuging is seen as darker regions. The brighter region, which still shows the presence of residual X-ray attenuating brine, represents tighter rock type.

Figure 2e shows the difference between the dry and the drained state images. This difference image can be segmented into an open (drained volumes) and a tight (volumes containing residual water) rock type, thus giving a 3D distribution of the open and the tight rock types within the plug. The segmented images are shown in figure 3. From these images we can see that the laminas are not perfectly horizontal. In sample 254 the open rock spans the entire height of the plug through a small connection in the middle of the sample. Later we will use this distribution of the open and tight rock types within the plug, populated with properties determined from the high resolution sub-plug scale images, to obtain effective properties at the plug scale. Sub-plugs of diameter 3 or 5 mm were cored from each plug to represent the open and the tight rock types, see figure 1.

The location of sub-plugs was chosen based on the drained image of the plug. The sub-plug representing open rock type was core from the brighter regions, while the tighter rock type was cored from the darker regions (ref figures 2&3). We also cored sister sub-plugs of open and tight rock types for porosity and MICP experiments, see figure 4. To minimize measurement errors these sister plugs were of larger diameter (9 mm) than the ones used for XCT imaging. Most of the tight lamina from sample 235 was damaged during extraction of the 3 mm sub-plug, so its sister sub-plug was extracted from near the top of the plug (figure 2). XCT imaging revealed that the sister sub-plug of 235 tight rock contained a significant amount of the open rock. Figure 4 shows the result of MICP experiments done on the sister sub-plugs. Both MICP experiments show a bimodal pore size distribution. The sister sub-plug of 235 tight contains a significant amount of open rock is reflected in its MICP curve and the presence of tight rock in the 235 open samples can also be seen from XCT images (figure 4). Our centrifuge speed corresponding to a throat size of 3 μm is then in good agreement with the MICP data indicating that the two rock types are separated by throat sizes in the range of 3-10 μm.

Porosity Estimation

Helium pycnometry was performed on the plugs at the beginning of the study, and also on the sister sub-plugs extracted to represent the open and tight rock types. Image based porosity was calculated by a "total-connected-porosity" segmentation technique described in Ghous *et. al.*, 2007. This segmentation approach is applied on the difference image (obtained by subtracting a dry from a saturated image) to determine both resolved (porous features larger than the voxel resolution) and sub-resolution porosity (see figure 5). Porosity was calculated using this segmentation approach both at the plug and from higher resolution images at the sub-plug scale. As seen in figure 2c, in the difference image of the plug (resolution 15.33 μm) the fluid signal in the tight lamina is faint (green inset) in comparison to the brighter signal from the open rock lamina (red inset), and more susceptible to underestimation due to the noise in the image, when processed as a single image. In order to minimize image processing errors, we have split the plug image into an open and tight part based on the drainage rock typing image. The open image contains only the open rock-type and the tight part masked and *vice versa* (figure 3). Each partial plug image was segmented separately, and resulting segmented images were combined to provide the porosity of the entire plug, as shown in the following sections. This allowed us decouple porosity of the open and tight rock types in the plug image. The results are shown in table 1.

Similarly, the high resolution sub-plug images (resolution ~3μm) were also segmented independently to determine the porosity of the open and the tight rock sub-plugs. By registering the high resolution sub-plug image into the low resolution plug image allowed for comparison of porosity from the matching volumes between the two images (see figure 5). For the tighter rock type, a significant amount of porosity could not be resolved even with the resolution of sub-plug image (see MICP in figure 4). Further investigation of the tight rock by SEM to probe the porosity microstructure (see figure 6) along with mineralogy derived by quantitative evaluation of minerals by scanning electron

microscopy (QEMScan) shows the presence of fine grained quartz kaolinite, illite/muscovite and large portion of organic matter which may not be fully saturated in the saturated image. We also see a significant presence of iron rich minerals such as chlorite, biotite, siderite and high attenuating X-ray trace minerals. These minerals often create artefacts in the CT image and could also be contributing towards the lower porosity estimations.

Permeability on sub-plugs

Two distinct approaches were used to determine permeability of the open and the tight rock types. Lattice-Boltzmann method (LBM) to simulate permeability on the open rock type, since this method can only be applied on the resolved pores, and, Katz-Thompson approach [Katz-Thompson, 1986] to estimate permeability where the connectivity is dominated by sub-resolution pore throats. The open rock sub-plugs showed connectivity of the resolved pores in the XCT image, and were suitable for Lattice-Boltzmann simulations. The LBM simulations were first run on the full image (1200^3 voxels) and also on the 400^3 voxel size subsets of the full image chosen at regular interval to capture the variability within the open rock sub-plug. Results are plotted in figure 7 and they show 5-10 porosity units variation within the subsets and an order of magnitude change in permeability. Anisotropy was observed in both samples, with vertical permeability an order of magnitude lower than the horizontal permeability. Also, the open regions of sample 235 were found to be more permeable than the respective regions of sample 254, which is consistent with the observation from the high resolution tomograms (see figure 7) that exhibits larger grain and pore sizes in sample 235 compared to 254. In case of the tight rock sub-plugs, the porosity obtained from the XCT image is mainly associated with either small pores or with secondary porosity not resolved in the XCT image.

In order to obtain an estimation of permeability on the tight sub-plug using the Katz-Thompson correlation, we first need to determine the critical aperture diameter. This is done in two steps. (1) Critical porosity fraction in 3D porosity map was obtained by starting with the resolved pores and adding progressively lower sub-resolution porosity fraction voxels (ref figure 5) to the porosity map till the pore space connects from the inlet to the outlet. (2) Critical porosity fraction were mapped on to the registered higher resolution 2D SEM, then an average of several pore throat diameters corresponding to the critical porosity fraction was measured and used as an estimate for critical aperture diameter. Porosity used in the equation below was obtained from the 3D difference image of tight sub-plug and cementation exponent was assumed to be equal to 2.

$$k = \frac{1}{32} l_c^2 \phi^m$$

$l_c = Critical\ \ Aperture\ \ Diameter$

$\phi = Porosity$

$m = Cementation\ \ Exponent$

The permeability results from both the open and the tight rock types are summarized in table 2.

Upscaling porosity and permeability to plug scale

The core plug CT scans were transformed to corner point grids (each cubic voxel is defined as a grid block with eight corners/nodes identified by *ijk* index) used in ECLISPE reservoir modeling software. These grids contained only two rock types as seen in figure 3 (2 different SATNUM only). Each grid cell then represents either the tight or the open rock type, and is associated with a distinct porosity and a permeability tensor. For each of the three directions, single phase up-scaling is done by assuming a pressure drop over the model in the given direction, and then solving the Darcy equation as described in Lopez *et. al.* 2012. This gives an upscaled permeability tensor for the 2 plug samples. Both permeability and porosity were upscaled to the core plug scale for comparison with available experimental data. The accuracy of porosity determined at the two scales of investigation (see figure 5) is compared in table 1, and shows a good match between the plug image and the open sub-plug image. However, the image based method underestimates porosity of the tight rock lamina, especially for sample 235 which has significant fraction of the plug as tight rock type and possible reasons for mismatch are discussed in the previous sections. Helium porosity results derived on the sister sub-plugs are also included in table 1. Due to the high degree of heterogeneity of these plugs, the representativeness of the sister sub-plugs used in this experiment was also tested using a quick XCT of the 9 mm sister samples used in the helium porosity measurement. Figure 4 reveals the presence of both open and tight rocks in sample 235 tight analogue, thus resulting in the higher helium porosity measurement and bimodal pore size distribution in the MICP.

Table 1: Porosity measured at different volumes in different images.

Sample	Fraction of rock type	Helium porosity	Sub-plug porosity (image)	Plug porosity (image)
235 Plug	-	**25.2**	-	**22.6**
235 open	0.39	32.4*	31.9	32.5
235 tight	0.61	27.4*	15.4	16.3
254 Plug	-	**32.8**	-	**31.8**
254 open	0.86	35.5*	32.0	32.4
254 tight	0.14	29.1*	27.3	28.4

**The values marked with an asterisk are from sister plugs.*

Permeability determined on each lamina along with the experimentally determined vertical permeability on the plug are summarized in table 2. Only vertical permeability was compared to experimental permeability as the plugs investigated are vertical plugs.

Table 2: Permeability measured and calculated for the different sub-plugs in all directions.

Sample	Fraction of rock type	Klinkenberg Permeability	Calculated permeability (mD) k_x	k_y	k_z

		(mD)			
235 Plug		**0.12**	-	-	**0.27 ***
235 open	0.39	-	1411	1417	217
235 tight	0.61	-	-	-	0.098
254 Plug		**3.25**	-	-	**17.7 ***
254 open	0.86	-	173	172	23
254 tight	0.14	-	-	-	5.15

** Upscaled core plug permeability based on open and tight lamina permeability*

Grids used in permeability upscaling simulation accurately represented the distribution of open and the tight rocks (figures 3 & 8) within the plug. In performing upscaling, we have used a single porosity and three permeabilities (kx, ky and kz, see table 2) to represent each, open and tight rock represented on the upscaling grid.

For sample 235, the vertical permeability was dominated by the tight rock and the resulting upscaled permeability shows a good match with the experimental results, considering three order of magnitude differences between the open and the tight rock permeability. We also note that the Katz-Thompson correlation used in obtaining permeability estimation on tight rock, does not take into account the effect on permeability from tortuosity or the effect from the size of pores other than the critical pore (Berg, 2014). The permeability for the tight lamina from the Katz-Thompson correlation was therefore viewed as uncertain, and when compared to the overall plug permeability with the experimental results, it was obviously too high.

For sample 254, the vertical permeability was dominated by the open rock, however the resulting upscaled permeability was significantly higher than the experimental one (17.7 mD and 3.25 mD respectively). The tight lamina does not have a significant effect on the upscaled permeability since the more permeable open rock percolates from the inlet to outlet of the plug as shown in figure 8. However, from the cross-plot of porosity and permeability of open rock type shown in figure 7, we can observe a 5-10 units of porosity variation and an order of magnitude variation in permeability within the same rock type. This local variation was not reflected in the single value of porosity and permeability tensor (see table 2) that was used in the upscaling simulation. In future work we will incorporates spatial porosity & permeability variation within each rock type; however this was beyond the scope of this study.

CONCLUSION

In this study, we demonstrate a novel method of mapping heterogeneity in complex reservoir rocks using a combination of digital rock analysis and experimental techniques. We also show a work flow for obtaining RCA properties from heteroneous core plugs.

Traditionally for heterolithic samples, the vertical permeability is associated to the permeability of the tightest lamina while the horizontal permeability is representing the most open lamina. In this study we have shown that the validity of such an assumption depends on the 3D lamina distribution inside the investigated core plugs and orientation of lamina. The proposed method to map heterogeneity can be applied to complex carbonates and also to capture more than two rock types by draining the plug to another capillary pressure.

Our upscaling grid captures the interplay between the open and tight lamina to the flow at the plug scale, however the accuracy of upscaled permeability could be improved by incorporating spatial porosity variation within each rock type.

ACKNOWLEDGEMENTS

The authors are grateful to Statoil ASA for permission to publish this paper. We would like to acknowledge Dr. Haili Long of FEI Norway for preliminary CT imaging and Prof. Mark Knackstedt of FEI Lithicon Digital Rock Services, Australia for fruitful discussions.

REFERENCES

1. Alberts, L., S. Bakke., P. Bhattad, A. Carnerup, M. Knackstedt, P.E. Øren, & B. Young, “Characterization of Unconventional Reservoir Core at Multiple Scales”, *Unconventional Resources Technology Conference, Denver, Colorado*, (Aug 2013).
2. Amaefule, J.O., M. Altunbay, D. Tiab, D.G. Kersey, & D.K. Keelan. “Enhanced reservoir description: using core and log data to identify hydraulic (flow) units and predict permeability in uncored intervals/wells”, *SPE Annual Technical Conference and Exhibition, Houston, Texas*, (Oct 1993).
3. Archie, G. E., “Classification of carbonate reservoir rocks and petrophysical considerations”, *AAPG Bulletin*, (1952) 36(2), 278-298.
4. Arns, C. H., F. Bauget, A. Ghous, A. Sakellariou, T.J. Senden, A.P. Sheppard & M.A. Knackstedt, “Digital core laboratory: Petrophysical analysis from 3D imaging of reservoir core fragments”, *Petrophysics,* (2005). 46(4) 260-277.
5. Berg, C.F., "Permeability Description by Characteristic Length, Tortuosity, Constriction and Porosity", *Transport in Porous Media*, (2014) 103(3), 381.
6. Ghous, A., T.J. Senden, R.M. Sok, A.P. Sheppard, V.W. Pinczewski, & M.A. Knackstedt, “3D characterization of microporosity in carbonate cores”, *SPWLA Middle East Regional Symposium in Abu Dhabi*, (Apr 2007).
7. Hamon, G., & M. Bennes, “Two-phase flow rock typing: another approach”, *Petrophysics*, (2004) 45(5), 433-444.
8. Hollis, C., V. Vahrenkamp, S. Tull, A. Mookerjee, C. Taberner, & Y. Huang, “Pore system characterisation in heterogeneous carbonates: An alternative

approach to widely-used rock-typing methodologies", *Marine and Petroleum Geology*, (2010) 27(4), 772-793.
9. Jackson, M.D., A.H. Muggeridge, S. Yoshida & H.D. Johnson "Upscaling permeability measurements within complex heterolithic tidal sandstones", *Mathematical Geology*, (2003) 35(5), 499-520.
10. Katz A.J. & A.H. Thompson, "Quantitative prediction of permeability in porous rock", *Physiscs. Review. B*, (1986) 34 (11), 8179
11. Latham, S., T. Varslot & A. Sheppard, "Image registration: Enhancing and calibrating X-ray micro-CT imaging", *SCA in Abu Dhahi*, (Nov 2008)
12. Lopez O., A. Mock, P.E. Øren, H. Long, Z. Kalam, V. Vahrenkamp, M. Gibrata, S. Seraj, S. Chacko, M. Al Hammadi, H. Al Hosni, H. Sahn & A. Vizamore, "Validation of fundamental carbonate reservoir core properties using digital rock physics", *SCA in Aberdeen, Scotland*, (Aug 2012)

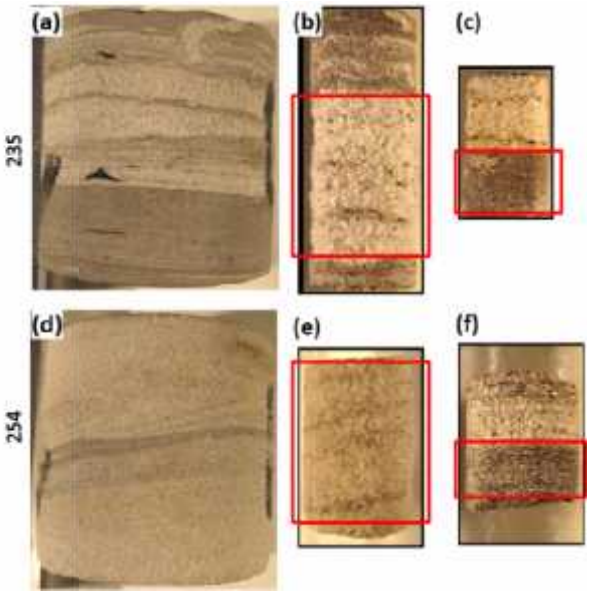

Figure 1: Photographs showing: (a&d) Laminated sandstone plugs (diameter=25mm) (b&e) Sub-plugs of 5 mm diameter extracted from open lamina (c) Sub-plug of 3 mm diameter extracted from tight lamina of sample 235 and (f) Sub-plug of 5 mm diameter extracted from tight lamina of sample 254. Imaging and analysis was performed only on the regions marked in red to capture properties of a single rock type.

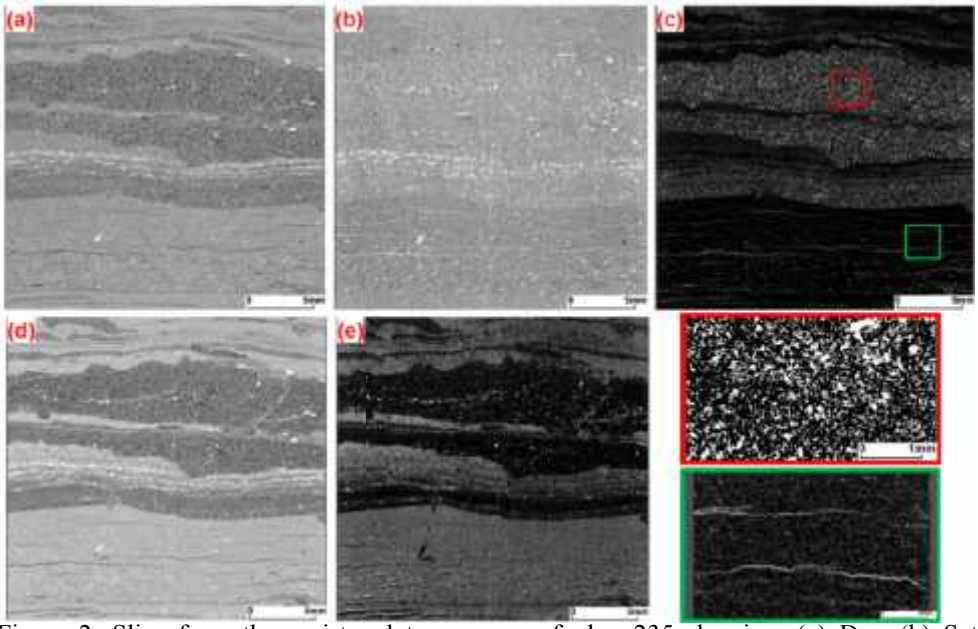

Figure 2: Slice from the registered tomograms of plug 235 showing: (a) Dry, (b) Saturated, (c)Total connected porosity with zoomed in view of high (red) and low (green) porosity regions, (d) after drainage by centrifuge and, (e) difference image showing Tight (brighter regions) and Open (darker regions) rock types, obtained by subtracting dry image from the drained image. Image resolution 15.33 μm/voxel.

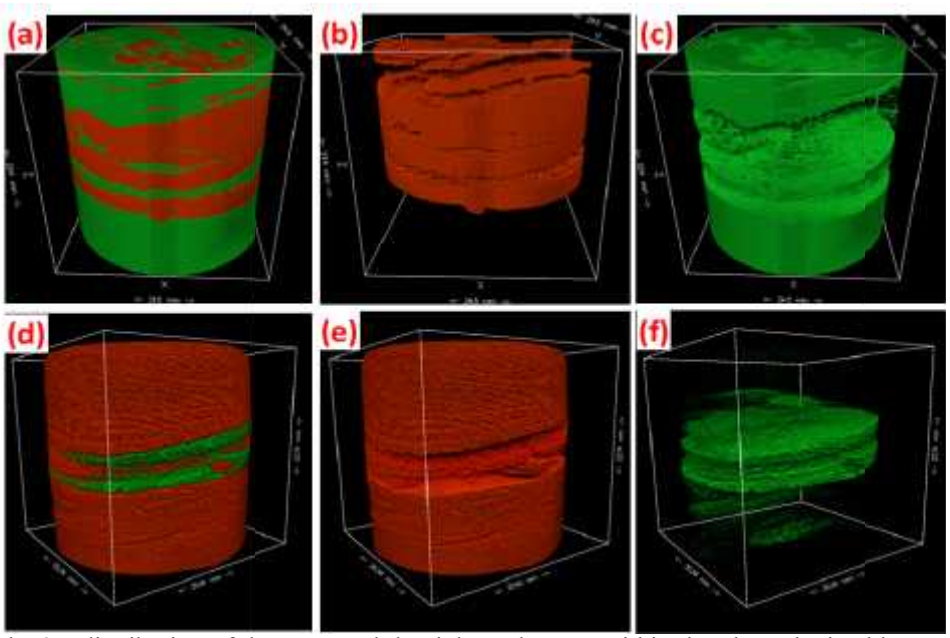

Figure 3: The 3D distribution of the open and the tight rock types within the plug, obtained by segmenting the resulting drained and residual volumes from centrifuging the plugs. The drained volume is assumed to represent the open rock type, while the residual volume represents the tight rock type.

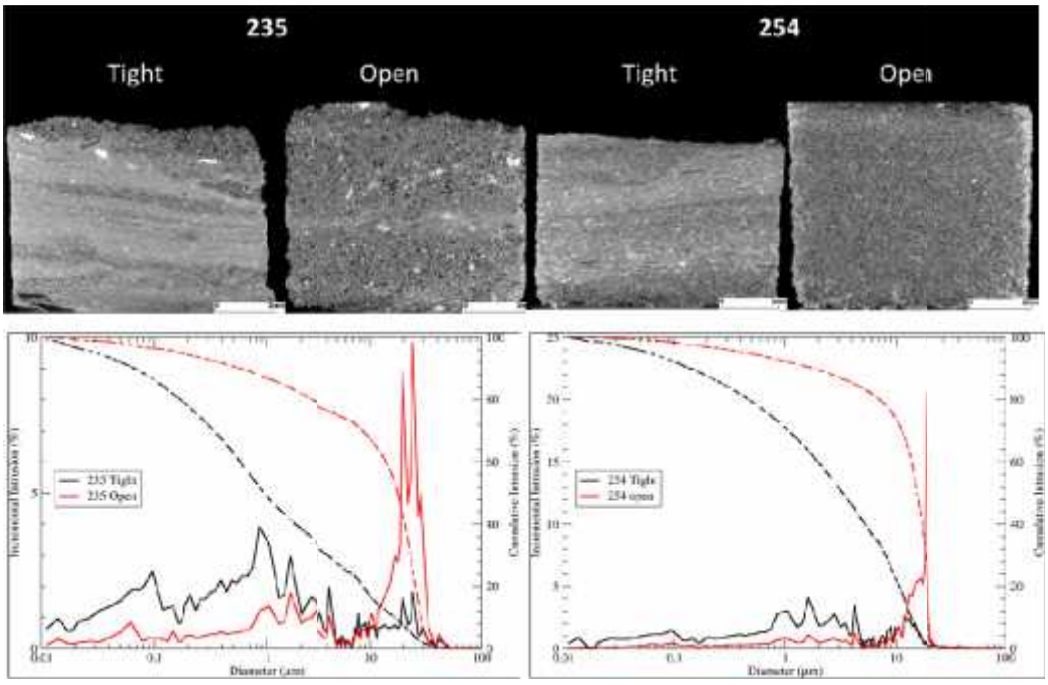

Figure 4: Sister sub-plug (9 mm diameter) cored form the plugs to represent open and tight rock types. **Top:** Quick XCT images showing representativeness of sister samples. **Bottom:** MICP curves on the sister sub-plugs, (Left) sample 235 and (Right) sample 254.

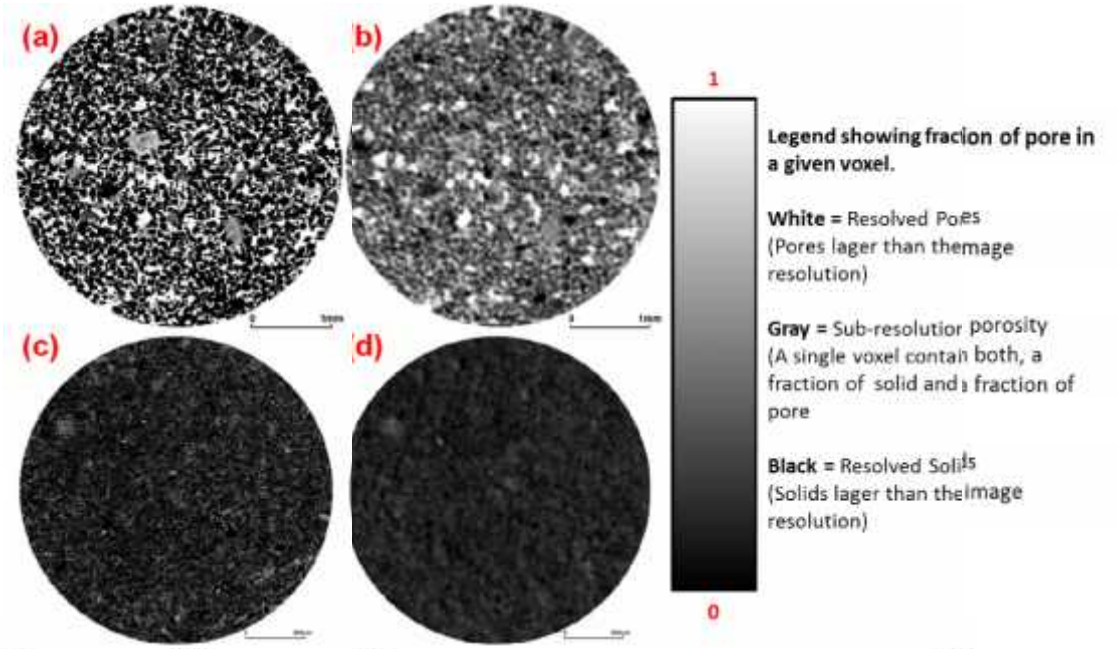

Figure 5: Comparison of total connected porosity estimated from the registered plug scale (voxel resolution 15.3 µm) and sub-plug scale image (voxel resolution 3.28 µm). **Open Lamina**: (a) Sub-plug image (ϕ=11.9%), (b) plug-scale image (ϕ=12.5%). **Tight Lamina:** (c) sub-plug scale image (ϕ= 5.4%), and (d) plug-scale image(ϕ= 6.2%).

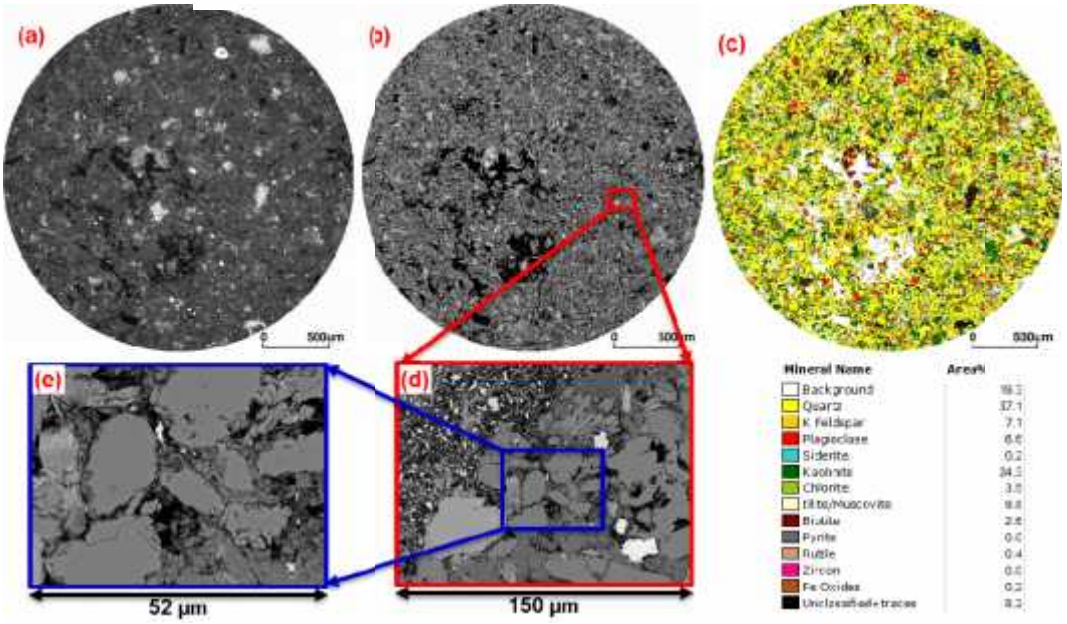

Figure 6: Registered XCT image and SEM of the tight rock type from sample 235. (a) Registered 2D section of the dry XCT image, (b) Registered 2D SEM and, (c) Registered QEMScan showing mineralogy of the sample, and high resolution SEM showing microstructures at (d) 2000X magnification and, (e) 6000X magnification.

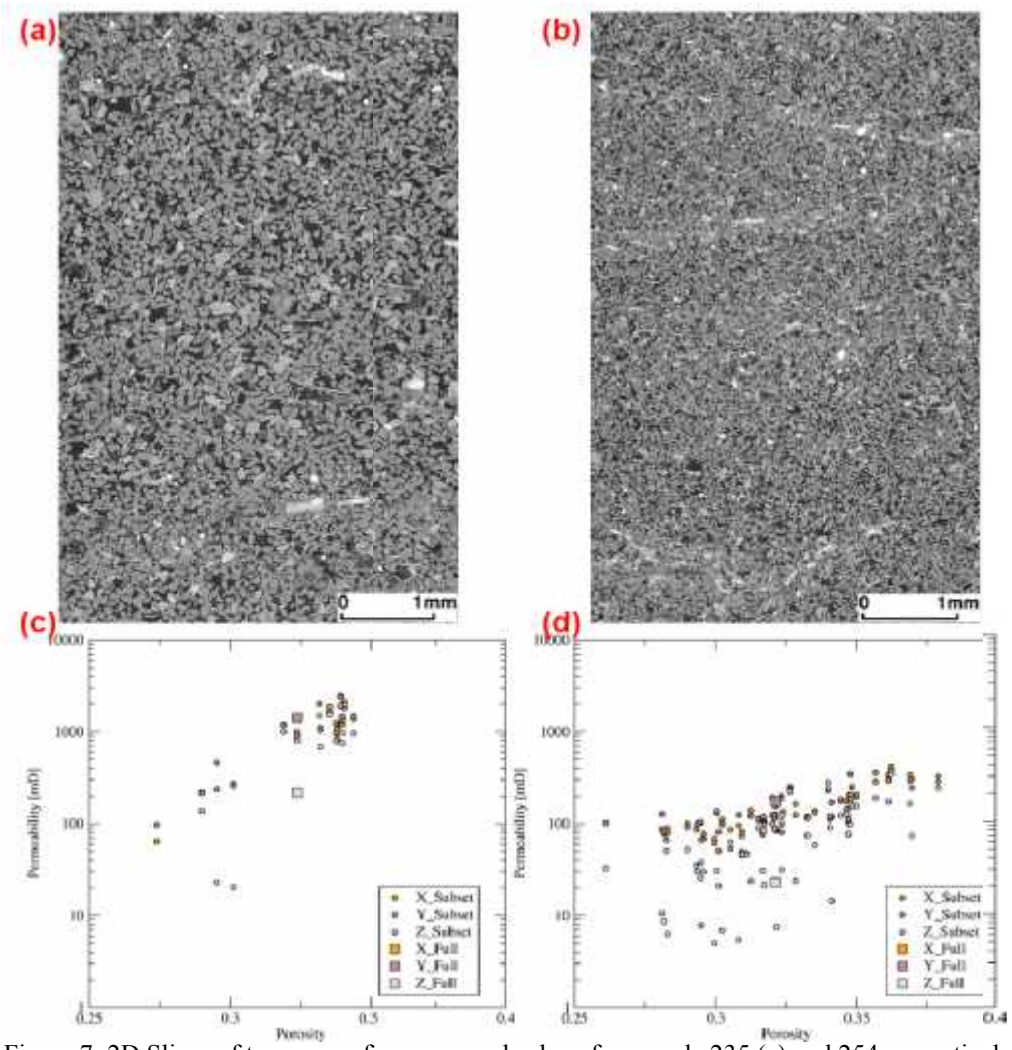

Figure 7: 2D Slices of tomogram from open sub-plugs for sample 235 (a) and 254 respectively (b) Porosity-Permeability cross plot calculated from open sub-plug of 235 (c) and 254 (d).

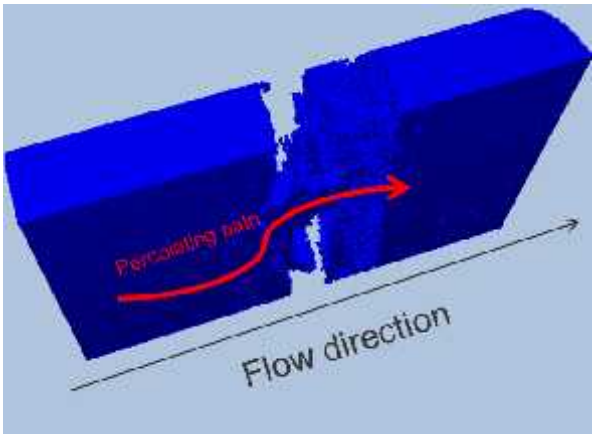

Figure 8: 3D distribution of open lamina showing a percolation path through sample 254